Polymer Chemistry

Accepted Manuscript

This is an *Accepted Manuscript*, which has been through the Royal Society of Chemistry peer review process and has been accepted for publication.

Accepted Manuscripts are published online shortly after acceptance, before technical editing, formatting and proof reading. Using this free service, authors can make their results available to the community, in citable form, before we publish the edited article. We will replace this *Accepted Manuscript* with the edited and formatted *Advance Article* as soon as it is available.

You can find more information about *Accepted Manuscripts* in the Information for Authors.

Please note that technical editing may introduce minor changes to the text and/or graphics, which may alter content. The journal's standard Terms & Conditions and the Ethical guidelines still apply. In no event shall the Royal Society of Chemistry be held responsible for any errors or omissions in this *Accepted Manuscript* or any consequences arising from the use of any information it contains.

ROYAL SOCIETY OF CHEMISTRY

www.rsc.org/polymers

Polymer Chemistry

ARTICLE

Title Effect of Side-Chain Halogenation on the Interactions of Conjugated Polymers with SWNTs†

Received 00th January 20xx,
Accepted 00th January 20xx

DOI: 10.1039/x0xx00000x

www.rsc.org/

M. Imit and A. Adronov[a]

Three fluorene-based π-conjugated copolymers, poly[(9,9'-dioctylfluorene)-*alt*-(9,9'-dihexylfluorene)] (**PFO-FH**), poly[(9,9'-dioctylfluorene)-*alt*-(9,9'-bis(6-bromohexylfluorene)] (**PFO-FHBr**), poly[(9,9'-dioctylfluorene)-*alt*-(9,9'-bis(6-iodohexylfluorene)] (**PFO-FHI**), which possess the same polymer backbones, were synthesized via Suzuki polycondensation. These three copolymers are practically identical in molecular structure and degree of polymerization. The only difference between them is the chain-end functionality of side-chains, which included hydrogen, bromine, and iodine, respectively. Each of these polymer structures was found to interact with the surface of single-walled carbon nanotubes (SWNTs), forming stable dispersions in organic solvents, such as THF. Using UV-Vis-NIR absorption, photoluminescence excitation (PLE) mapping, and Raman spectroscopy, it was found that the terminal atom of the polymer side-chains influenced the specific SWNT chiralities that were dispersed by the polymer.

Introduction

Single-walled carbon nanotubes (SWNTs)[1,2] are among the most widely investigated nano-scale materials of the 21st century. Their unique chemical,[3] mechanical,[2,4] optical,[5,6] and electronic properties make them potentially useful for various electronic and optical devices,[6,7] nanostructured materials,[8] functional composites,[9,10] printable electronics,[11–14] and bio-medical applications.[15] However the co-existence of tubes having various diameters and chiralities in commercially available SWNT samples, with the concomitant differences in electrical conductivity (ranging from semiconducting to metallic), has been detrimental for fundamental research and fabrication of high-performance SWNT-based devices.[16,17] It is clear that removal of impurities, separation of metallic and semiconducting SWNTs, and sorting SWNTs according to their diameter, chirality, and length are important research pursuits that will enable broader nanotube penetration in device applications.[17,18]

In recent years, several methods for nanotube purification and enrichment of specific semiconducting chiralities have been demonstrated, including density gradient ultracentrifugation (DGU),[16,17] gel filtration,[17,19] dielectrophoresis,[20] aqueous two-phase extraction,[21,22] and selective extraction using conjugated polymers.[23,24] Although each technique has its own unique advantages and provides comparatively reliable routes to enrichment of semiconducting SWNTs (sc-SWNTs), the relative simplicity of the π-conjugated polymer extraction process makes it a cost-effective and scaleable method for sc-SWNT isolation.[24,25] Research in this area began with reports of non-covalent functionalization of SWNTs using π-conjugated polyfluorenes, such as poly(9,9'-dioctylfluorene) (PFO)[26,27] and poly(9,9'-didodecylfluorene) (PDDF),[28,29] as well as fluorene containing copolymers,[30,31] which demonstrated excellent dispersions and highly enriched samples of sc-SWNTs in aqueous and organic media. Subsequent progress extended the scope of conjugated polymers to polythiophenes,[32] poly(*p*-phenylene ethynylenes),[33] polycarbazoles,[34,35] and a number of derivative structures.[23,36] Furthermore, several reports have described the effect of conjugated polymer structure,[37,38] molecular weight[39,40] solvent effects,[41] sonication conditions,[41,42] and side-chain structure (including alkyl group architecture and length)[43,44] on the selectivity toward dispersion of specific SWNT chiralities. These studies have shown that small changes in polymer structure can result in dramatic changes in the nanotube chiralities that are selectively dispersed in solvents. However, a detailed understanding of the important parameters that can be modified to bias nanotube dispersions to specific chiralities has not been developed, partly because multiple variables (molecular weight, structure, electronics, side-chain functionality) confound the interpretation of dispersion results, and prevent fundamental understanding.

In an attempt to elucidate the effect of small changes in side-chain functionality on the dispersion selectivity of polyfluorenes toward SWNTs, we have prepared three alternating copolymers of equivalent molecular weight comprising 9,9'-dioctylfluorene copolymerized with 9,9'-dihexylfluorene, 9,9'-bis(6-bromohexyl)fluorene, and 9,9'-bis(6-iodohexyl)fluorene. We show that the simple

[a] *Department of Chemistry, McMaster University, 1280 Main St. W., Hamilton, ON, Canada, L9S 4M1.*

† Electronic Supplementary Information (ESI) available: Full experimental details, as well as NMR spectra of monomers and polymers, and fluorescence data for polymer-SWNT complexes. See DOI: 10.1039/x0xx00000x

modification of polymer side-chains with halogens produces little change in the overall physical properties of the polymers, but has a significant influence on the SWNT chiralities that are dispersed in organic solvent.

Results and Discussion

Synthesis and Characterization of Polymers.

All monomers were either purchased from commercial sources or prepared according to literature procedures (Scheme 1). Preparation of 9,9'-dihexyl-2,7-diiodofluorene (2) and 9,9'-bis(6-bromohexyl)-2,7-diiodofluorene (3) involved electrophilic iodination of fluorene followed by attachment of the solubilizing alkyl chains via nucleophilic substitution under phase-transfer conditions.[45,46] 9,9'-bis(6-iodohexyl)-2,7-diiodofluorene (4) was readily prepared from 3 using halogen exchange with sodium iodide in quantitative yield.[47] Polymerizations were carried out using Suzuki-Miyaura cross-coupling polymerization between 9,9'-dioctylfluorene-2,7-diboronic acid bis(1,3-propanediol) ester and each of the comonomers, 2, 3, and 4 (Scheme 1).[48,49] The resulting three copolymers, poly[(9,9'-dioctylfluorene)-*alt*-(9,9'-dihexylfluorene)] (PFO-FH), poly[(9,9'-dioctylfluorene)-*alt*-(9,9'-bis(6-bromohexylfluorene))] (PFO-FHBr), and poly[(9,9'-dioctylfluorene)-*alt*-(9,9'-bis(6-iodohexylfluorene))] (PFO-FHI), exhibited good solubility in common organic solvents, such as THF, toluene, and chloroform, enabling their complete characterization. Gel permeation chromatography (GPC) indicated that all three polymers had a number average molecular weight (M_n) of approximately 10 kDa and polydispersity index (PDI) values of approximately 3 (Table 1).[39,40,50] Representative ^{1}H NMR data for monomer 4 and the corresponding copolymer, PFO-FHI, is provided in Figure 1. This data clearly indicates that the iodohexyl-functionalized commoner is incorporated within the polymer structure, with preservation of the iodomethyl functionality in the side-chains,

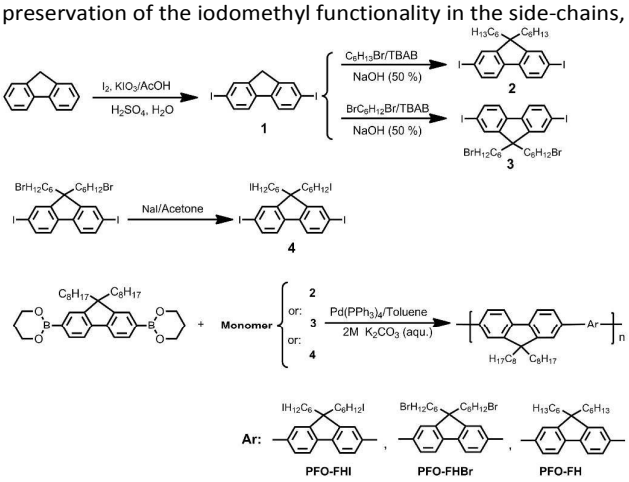

Scheme 1. Synthesis of the copolymers PFO-FH, PFO-FHBr, and PFO-FHI.

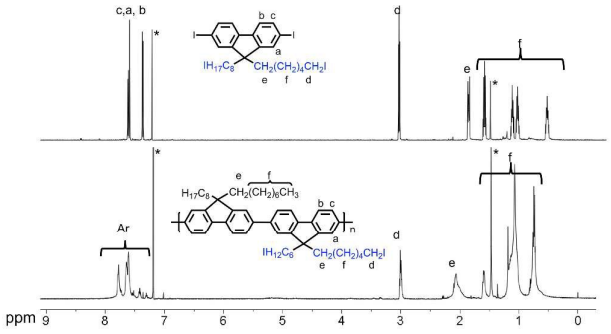

Figure 1. ^{1}H NMR spectra of the monomer **4** (top) and its copolymer **PFO-FHI** (bottom) in $CDCl_3$. Signals marked with an asterisk arise from $CHCl_3$ (~7.26 ppm) and water (~1.54 ppm).

which exhibits a chemical shift of 3.08 ppm. Similar data was collected for PFO-FHBr and PFO-FH (see Figure S2 and S3 in the Supporting Information).

Photophysical properties of the polymers were characterized by UV-Vis and fluorescence spectroscopy (Figure 2a). The absorption spectra were normalized and their corresponding emission spectra were corrected using the absorption normalization factors. The absorption spectra for all three copolymers were practically identical, with very small differences in their absorption maximum (λ_{max}) values. Interestingly, the extinction coefficient was found to be identical for **PFO-FH** and **PFO-FHBr**, with a value of approximately 6.5 × 10^4 $M^{-1}\cdot cm^{-1}$, but was nearly 35% higher for **PFO-FHI**. Similarly, the emission spectra for the three polymers were nearly identical from the perspective of peak position, but the emission intensity increased upon halogenation of the side-chain, with the highest intensity for **PFO-FHI**. The exact origin of these small differences in absorption and emission properties is not clear.

Thermogravimetric analysis (TGA) was used to evaluate the thermal stabilities of the three copolymers (Figure 2b). The TGA curve for **PFO-FH** shows a single decomposition event, with an onset of approximately 420 °C and a magnitude of nearly 50% of the original mass. This is consistent with the thermal decomposition of the alkyl side-chains of the polymer structure. For **PFO-FHBr** and **PFO-FHI**, two distinct decomposition events are observed, with the first having an onset of 300 and 310 °C, respectively, followed by a second decomposition that matches the onset temperature for that of **PFO-FH**. It can be concluded that the first decomposition event corresponds to the elimination of HX (X = Br or I), which is expected to occur at a lower temperature than the decomposition of the alkyl chains. The loss of the remaining alkyl chains occurs subsequently, at the same temperature as observed for **PFO-FH**. The magnitude of the calculated weight loss for each of these events is consistent with the proposed decompositions.

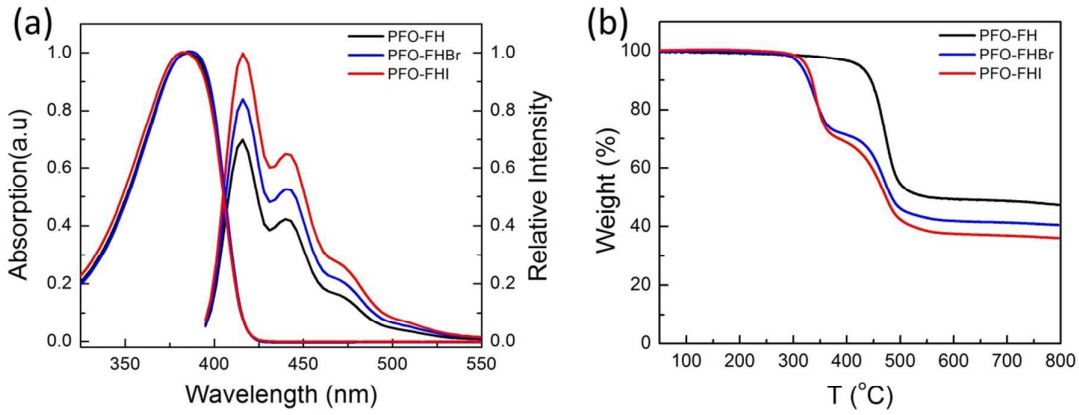

Figure 2. (a) UV-Vis and PL spectra of the copolymers in THF. Absorption spectra were normalized and emission spectra were corrected using the absorption normalization factors. (b) TGA curves for copolymers with a heating rate of 10 °C/min under Ar atmosphere.

Table 1. Molecular weight and optical properties of the copolymers.

Polymers	*M_n (Kg/mol)	PDI	UV-Vis (λ_{max}, nm)	ε_{max} ($M^{-1}\cdot cm^{-1}$) ($\times 10^{-4}$)
PFO-FHI	9.8	3.0	383	8.8 ±0.4
PFO-FHBr	10.2	3.4	386	6.4 ±0.4
PFO-FH	9.6	3.0	386	6.7 ±0.1

*Values obtained by GPC relative to polystyrene standards.

Supramolecular Polymer-SWNT Complexes.

The supramolecular interactions between these copolymers and HiPco SWNTs were investigated according to our previously reported methods.[51,52] In a typical experiment, a SWNT sample (2.5 mg) was added to a solution of polymer in THF (7.5 mg in 10 mL), and then the mixture was bath sonicated at 0 ºC for one hour. The resulting black suspension was centrifuged for 35 min at 8,300 *g*, and the supernatant was filtered through a 200 nm pore size Teflon membrane and washed with THF until no fluorescence could be detected from the filtrate under irradiation with a hand-held UV lamp at 365 nm. Then, the black residue was re-dispersed in 10 mL of THF via bath sonication, followed by a second centrifugation (25 min, 8,300 g) to ensure that the polymer-SWNT material is successfully re-suspended and the insoluble materials are removed. The resulting samples were extremely dark, stable dispersions in THF, regardless of the polymer that was used.

In order to determine if selective dispersion of carbon nanotubes was occurring, UV-Vis-NIR absorption spectroscopy absorption spectrum exhibited features that corresponded to was initially used to characterize the copolymer-SWNT complexes dispersed in THF. An aqueous (D_2O) solution of the first (S_{11}) and second (S_{22}) interband transitions for semiconducting tubes, which are found from 900 to 1600 nm SWNTs dispersed with SDBS, a non-selective dispersant of nanotubes, was used as a reference.[53] The UV-Vis-NIR and 600 to 900 nm, respectively (Figure 3a). Compared to the non-selective SWNT dispersion with SDBS, the polymer-SWNT samples produced well-resolved SWNT signals, indicating that the polymers can selectively disperse specific SWNT chiralities in THF. Interestingly, the observed spectral features were different, depending on the side chain functionality of the copolymers. **PFO-FH** has a strong tendency to disperse (7,5) and (8,6) nanotubes in THF, whereas PFO-FHI and PFO-FHBr mainly exhibit selectivity for four different SWNT species, including the (7,5), (7,6), (8,6) and (8,7) chiralities. The overlaid fluorescence spectra of the three polymer-SWNT dispersions and the non-selective SDBS-SWNT dispersion in D_2O, recorded with excitation at 550 nm, are depicted in Figure 3b (for clarity, the figure without SDBS-SWNT is available in the supporting information). This data shows that the polymer-SWNT dispersions exhibit fewer emission peaks, which have a much sharper lineshape, compared to the SDBS-SWNT dispersion. This emission data is consistent with the observed absorption spectra, with **PFO-FH** exhibiting strong selectivity for the (7,5) and (8,6) SWNT chiralities, while **PFO-FHBr** and **PFO-FHI** both showing selectivity for the (7,5), (7,6), (8,6) and (8,7) chiralities. However, it should be noted that the intensity of the PLE and UV-Vis-NIR absorption peaks can vary with differences in molar extinction coefficient and fluorescence quantum yield of each individual polymer-SWNT combination, making it difficult to correlate peak intensity with concentration.[54–56]

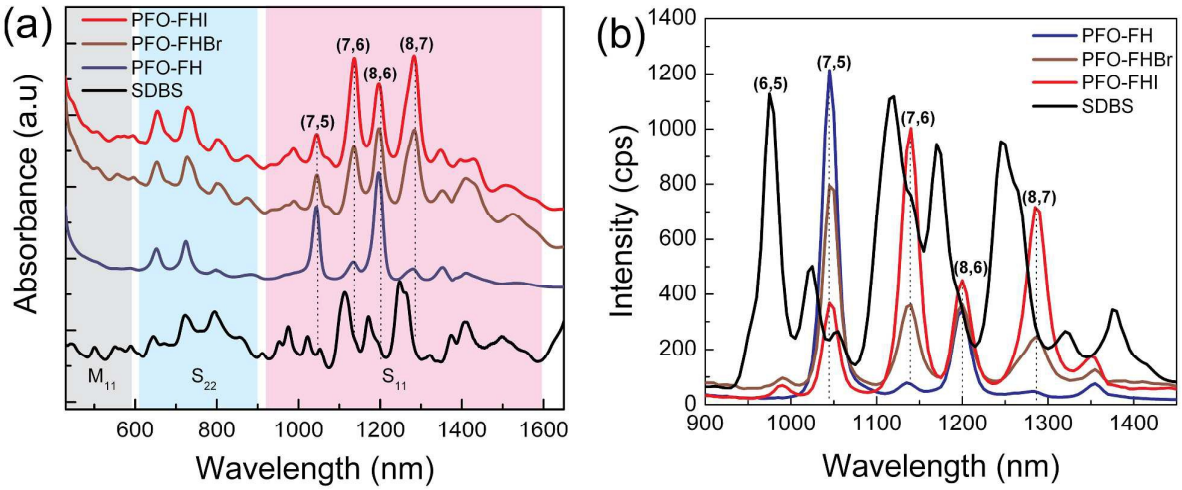

Figure 3. (a) Comparison of UV–Vis–NIR absorbance data for the SDBS-SWNT dispersion in D2O with the PFO-FHI-SWNT, PFO-FHBr-SWNT, and PFO-FH-SWNT dispersions in THF; absorbance traces have been vertically offset for clarity. (b) Comparison of fluorescence signal intensity using an excitation wavelength of 550 nm for the SDBS-SWNT dispersion in D2O with the PFO-FHI-SWNT, PFO-FHBr-SWNT, and PFO-FH-SWNT dispersions in THF.

Photoluminescence excitation maps (PLE) of the samples were measured over a large range of excitation and emission wavelengths (500-850 nm and 900-1450 nm, respectively). Since the absorption (E_{22}) and emission (E_{11}) wavelengths of semiconducting SWNTs vary with nanotube chirality, PLE maps allow identification of the nanotube species present within a dispersion. Figure 4 compares the PLE maps of **PFO-FH**-SWNT, **PFO-FHBr**-SWNT, and **PFO-FHI**-SWNT dispersions in THF with the PLE map of an aqueous SWNT dispersion using SDBS. High emission intensities are represented in red and low intensities are represented in blue. The chiral indices (n, m) for the identified SWNT species are labeled on the corresponding maps according to previously reported assignments.[16,57] This PLE data shows that the polymer-SWNT dispersions give rise to intense fluorescence from individual sc-SWNT chiralities, which can only occur if nanotube bundles are effectively exfoliated by these polymers. Furthermore, the number of nanotube species dispersed by the polymers is dramatically lower than what is observed with SDBS, indicating that all three copolymers exhibit selectivity for specific nanotube chiralities. As was observed from the UV-Vis-NIR absorption spectra, **PFO-FH** is selective for two major SWNT species, the (7,5) and (8,6), while **PFO-FHBr** and **PFO-FHI** selectively disperse four major species, including (7,5), (7,6), (8,6), and (8,7). It is interesting to note that a simple substitution of a hydrogen atom with a halogen at the chain end of the polymer side-chains has a significant impact on the nanotube chiralities that are dispersed. Figure 5 shows the relative PLE intensity from the different nanotube species dispersed by each polymer. The most intense signal from each solution was normalized to 1 and the nanotube species are organized by diameter, which ranges from 0.829 nm for the (7,5) tube to 1.032 nm for (8,7) tube. It can be seen that use of **PFO-FH** and **PFO-FHBr** resulted in the highest emission intensity from the (7,5) chirality, while use of **PFO-FHI** resulted in the highest emission intensity from the (7,6). Additionally, the halogenated polymers resulted in significant emission from (8,6) and (8,7) SWNTs, possibly indicating some preference for dispersing higher diameter nanotubes. Most likely, the introduction of electronegative and polarizable halogens in the polymer side chains imparts greater surface charge to the polymer-SWNT complexes and results in better electrostatic stabilization of the colloidal dispersion produced in THF. This enables stable dispersion of high concentrations of SWNTs, even for the larger-diameter SWNTs that are generally more difficult to disperse. In addition, the extra colloidal stability results in a decrease in the selectivity for specific SWNT chiralities.

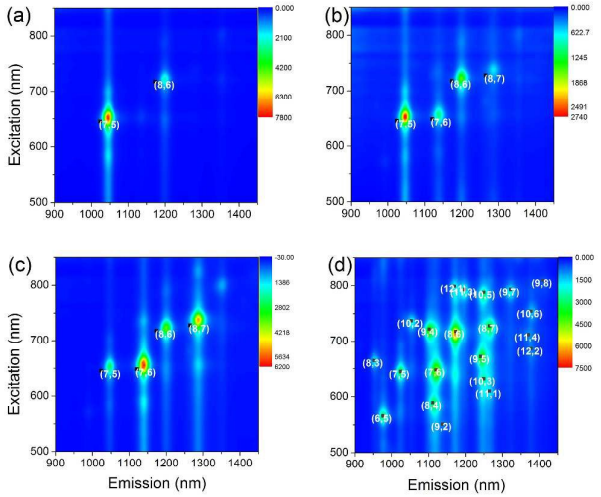

Figure 4. PL contour maps of HiPco SWNTs dispersed with copolymers **PFO-FH** (a), **PFO-FHBr** (b), and **PFO-FHI** (c) in THF, as well as with SDBS (d) in D_2O.

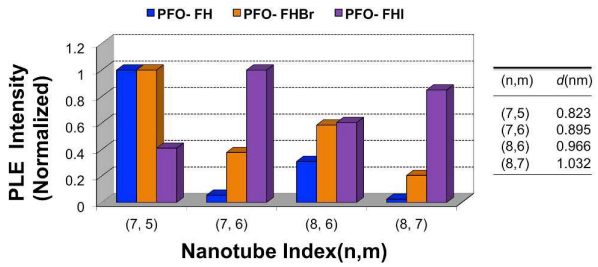

Figure 5. Normalized PLE signal intensities of the major SWNT species observed in THF solution of PFO-FH + SWNT(blue), PFO-FHBr + SWNT(orange), PFO-FH + SWNT(violet), respectively. Horizontal axis is in order of increasing diameter (left to right). The table on the right gives chiralities and their corresponding diameter (d, nm).

Resonance Raman spectroscopy is another useful tool for characterizing the composition of carbon nanotube samples. Using different excitation wavelengths, this technique enables differentiation of the electronic nature of nanotubes within different samples. We carried out Raman measurements, using excitation wavelengths of 785 nm and 633 nm (Figure 6), normalizing all the spectra to the graphitic band (G-band) at ~1590 cm^{-1}. The signals in the low-frequency range (100-400 cm^{-1}), referred to as the radial breathing modes (RBMs) are particularly indicative of both the nanotube types and diameters present in the samples. Excitation of the samples at 785 nm (Figure 6, a and b) results in signals emanating primarily from sc-SWNTs, which are in resonance with this wavelength. Comparing the spectrum from pristine HiPco SWNTs with that of the polymer-functionalized SWNTs, it can be seen that the signal at 265 cm^{-1}, which arises from (10,2) SWNTs that are bundled, has significantly diminished in the latter samples, indicating that polymer functionalization effectively exfoliates the nanotube bundles into individual nanotubes. Comparison of the three polymer-dispersed SWNTs shows little difference, with three dominant RBM signals between 231 and 245 cm^{-1}, arising from the (8,7), (8,6) and (7,6) nanotubes, respectively.[58,59] Excitation of the samples at 633 nm gives rise to RBM signals from both semiconducting (230-300 cm^{-1}) and metallic (175-230 cm^{-1}) SWNTs. These spectra indicate that the pristine SWNT sample contains both metallic and semiconducting nanotubes in the expected proportions. Interestingly, the two halogenated polymer-SWNT samples also exhibit signals corresponding to a mixture of m-SWNTs and sc-SWNTs. However, the spectrum for the **PFO-FH**-SWNT sample is dominated by a single peak at 284 cm^{-1}, which corresponds to the (7,5) semiconducting nanotube.[59,60] This data supports the previous observations that **PFO-FH** is extremely selective for a very narrow subset of sc-SWNTs, and can disperse these structures to a high concentration in THF.

Conclusions

Three fluorene-based π-conjugated polymers, **PFO-FH**, **PFO-FHBr** and **PFO-FHI** have been synthesized using Suzuki polycondensation, and the resulting polymers exhibited good solubility in a number of organic solvents, including THF, toluene, and chloroform. Thermogravimetric analysis indicated

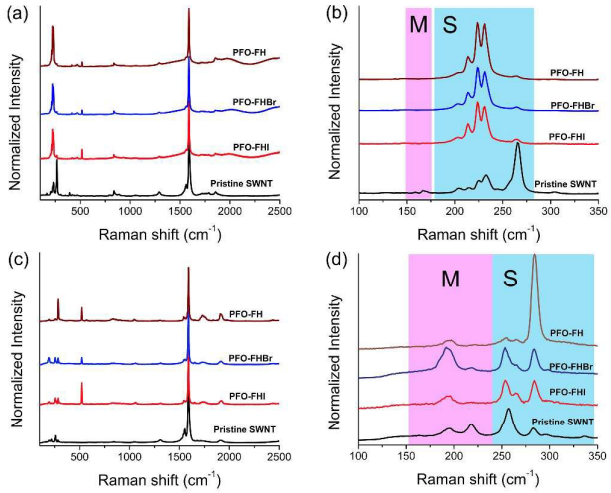

Figure 6. Raman spectra of HiPco SWNTs dispersed with copolymers **PFO-FH**, **PFO-FHBr**, and **PFO-FHI** in THF. Sample spectra in (a) were recorded with 785 nm excitation, while those in (c) were recorded with 633 nm excitation. The corresponding RBM regions are depicted in (b) and (d). Pink highlights correspond to RBM regions where signals from metallic (M) nanotubes arise and green highlights correspond to regions where signals from semiconducting (S) nanotubes arise.

that these copolymers exhibit excellent thermal stability under Ar. These copolymers were utilized for the preparation of supramolecular polymer-SWNT composites, and excellent nanotube solubility and solution stability was achieved in THF. UV-Vis-NIR absorption measurements and PLE mapping revealed that these copolymers have different affinity toward SWNTs in THF. In particular, **PFO-FH** exhibited a high degree of selectivity toward (7,6) and (8,6) SWNTs. Halogenation of side-chain functionalities resulted in relatively little impact on polymer structure and conformation, but had a significant effect on the selectivity of the polymers in dispersing specific SWNT structures.

Acknowledgements

Financial support for this work was provided by the National Science and Engineering Research Council of Canada (NSERC), the NSERC Photovoltaic Innovation Network, and the Canada Foundation for Innovation (CFI).

Notes and references

1 P. M. Ajayan, *Chem. Rev.*, 1999, **99**, 1787–1800.
2 H. J. Dai, *Acc. Chem. Res.*, 2002, **35**, 1035–1044.
3 M. S. Strano, A. A. Boghossian, W. J. Kim, P. W. Barone, E. S. Jeng, D. A. Heller, N. Nair, H. Jin, R. Sharma and C. Y. Lee, *MRS Bull.*, 2009, **34**, 950–961.
4 J. Z. Liu, Q. S. Zheng, L. F. Wang and Q. Jiang, *J. Mech. Phys. Solids*, 2005, **53**, 123–142.
5 Z. Chen, X. Zhang, R. Yang, Z. Zhu, Y. Chen and W. Tan, *Nanoscale*, 2011, **3**, 1949–1956.

6 P. Avouris, M. Freitag and V. Perebeinos, *Nat. Photonics*, 2008, **2**, 341–350.
7 X. Y. Sun and Y. G. Sun, *J. Mater. Sci. Technol.*, 2008, **24**, 569–577.
8 J. Lopez-Andarias, J. Luis Lopez, C. Atienza, F. G. Brunetti, C. Romero-Nieto, D. M. Guldi and N. Martin, *Nat. Commun.*, 2014, **5**.
9 J. T. Di, X. Wang, Y. J. Xing, Y. Y. Zhang, X. H. Zhang, W. B. Lu, Q. W. Li and Y. T. T. Zhu, *Small*, 2014, **10**, 4606–4625.
10 X.-Q. Liu, Y.-L. Li, Y.-W. Lin, S. Yang, X.-F. Guo, Y. Li, J. Yang and E.-Q. Chent, *Macromolecules*, 2013, **46**, 8479–8487.
11 R. P. Tortorich and J.-W. Choi, *Nanomaterials*, 2013, **3**, 453–468.
12 X. F. Guo, *Adv. Mater.*, 2013, **25**, 3397–3408.
13 S. Ghosh, S. M. Bachilo and R. B. Weisman, *Nat. Nanotechnol.*, 2010, **5**, 443–450.
14 F. Bonaccorso, *Int. J. Photoenergy*, 2010.
15 L. M. Liu, W. E. Stanchina and G. Y. Li, *Appl. Phys. Lett.*, 2009, **94**.
16 H. P. Liu, T. Tanaka, Y. Urabe and H. Kataura, *Nano Lett.*, 2013, **13**, 1996–2003.
17 H. Peng, N. T. Alvarez, C. Kittrell, R. H. Hauge and H. K. Schmidt, *J. Am. Chem. Soc.*, 2006, **128**, 8396–8397.
18 J. A. Fagan, C. Y. Khripin, C. A. Silvera Batista, J. R. Simpson, E. H. Hároz, A. R. Hight Walker and M. Zheng, *Adv. Mater.*, 2014, **26**, 2800–2804.
19 G. Ao, C. Y. Khripin and M. Zheng, *J. Am. Chem. Soc.*, 2014, **136**, 10383–10392.
20 S. K. Samanta, M. Fritsch, U. Scherf, W. Gomulya, S. Z. Bisri and M. A. Loi, *Acc. Chem. Res.*, 2014, **47**, 2446–2456.
21 P. Bilalis, D. Katsigiannopoulos, A. Avgeropoulos and G. Sakellariou, *RSC Adv.*, 2014, **4**, 2911–2934.
22 H. W. Lee, Y. Yoon, S. Park, J. H. Oh, S. Hong, L. S. Liyanage, H. L. Wang, S. Morishita, N. Patil, Y. J. Park, J. J. Park, A. Spakowitz, G. Galli, F. Gygi, P. H. S. Wong, J. B. H. Tok, J. M. Kim and Z. A. Bao, *Nat. Commun.*, 2011, **2**.
23 P. Lukaszczuk, E. Borowiak-Palen, M. H. Rummeli and R. J. Kalenczuk, *Phys. Status Solidi B-Basic Solid State Phys.*, 2009, **246**, 2699–2703.
24 A. Nish, J. Y. Hwang, J. Doig and R. J. Nicholas, *Nat. Nanotechnol.*, 2007, **2**, 640–646.
25 P. Imin, F. Y. Cheng and A. Adronov, *Polym. Chem.*, 2011, **2**, 411–416.
26 J. F. Ding, Z. Li, J. Lefebvre, F. Y. Cheng, G. Dubey, S. Zou, P. Finnie, A. Hrdina, L. Scoles, G. P. Lopinski, C. T. Kingston, B. Simard and P. R. L. Malenfant, *Nanoscale*, 2014, **6**, 2328–2339.
27 R. M. Si, L. Wei, H. Wang, D. D. Su, S. H. Mushrif and Y. Chen, *Chem. Asian J.*, 2014, **9**, 868–877.
28 M. Tange, T. Okazaki and S. Iijima, *ACS Appl. Mater. Interfaces*, 2013, **4**, 6458–6462.
29 H. L. Wang, J. G. Mei, P. Liu, K. Schmidt, G. Jimenez-Oses, S. Osuna, L. Fang, C. J. Tassone, A. P. Zoombelt, A. N. Sokolov, K. N. Houk, M. F. Toney and Z. A. Bao, *ACS Nano*, 2013, **7**, 2659–2668.
30 J. Mao, O. Liu, S. Wang, X. Lv, Y. Huang, Y. F. Ma, Y. S. Chen and S. G. Yin, *J. Nanosci. Nanotechnol.*, 2008, **8**, 3343–3350.
31 N. A. Rice and A. Adronov, *J. Polym. Sci. Part A-Polymer Chem.*, 2014, **52**, 2738–2747.
32 F. A. Lemasson, T. Strunk, P. Gerstel, F. Hennrich, S. Lebedkin, C. Barner-Kowollik, W. Wenzel, M. M. Kappes and M. Mayor, *J. Am. Chem. Soc.*, 2011, **133**, 652–655.
33 F. M. Chen, B. Wang, Y. Chen and L. J. Li, *Nano Lett.*, 2007, **7**, 3013–3017.
34 T. Fukumaru, F. Toshimitsu, T. Fujigaya and N. Nakashima, *Nanoscale*, 2014, **6**, 5879–5886.
35 N. Berton, F. Lemasson, A. Poschlad, V. Meded, F. Tristram, W. Wenzel, F. Hennrich, M. M. Kappes and M. Mayor, *Small*, 2014, **10**, 360–367.
36 P. Imin, F. Y. Cheng and A. Adronov, *Polym. Chem.*, 2011, **2**, 1404–1408.
37 F. Jakubka, S. P. Schießl, S. Martin, J. M. Englert, F. Hauke, A. Hirsch and J. Zaumseil, *ACS Macro Lett.*, 2012, **1**, 815–819.
38 Q. Cheng, S. Debnath, E. Gregan and H. J. Byrne, *J. Phys. Chem. C*, 2010, **114**, 8821–8827.
39 H. B. Yu, S. Hermann, S. E. Schulz, T. Gessner, Z. L. Dong and W. J. Li, *Chem. Phys.*, 2012, **408**, 11–16.
40 P. Gerstel, S. Klumpp, F. Hennrich, A. Poschlad, V. Meded, E. Blasco, W. Wenzel, M. M. Kappes and C. Barner-Kowollik, *ACS Macro Lett.*, 2014, **3**, 10–15.
41 H. L. Wang, G. I. Koleilat, P. Liu, G. Jimenez-Oses, Y. C. Lai, M. Vosgueritchian, Y. Fang, S. Park, K. N. Houk and Z. N. Bao, *ACS Nano*, 2014, **8**, 2609–2617.
42 W. Zeng, S. Liu, H. Zou, L. Wang, R. Beuerman and D. Cao, *J. Polym. Sci. Part A-Polymer Chem.*, 2010, **48**, 4168–4177.
43 Q. Wang, M. Huang, Y. Huang, J. S. Zhang, G. F. Zhou, R. Q. Zeng and X. B. Yang, *Med. Chem. Res.*, 2014, **23**, 2659–2666.
44 D. Stay and M. C. Lonergan, *Macromolecules*, 2013, **46**, 4361–4369.
45 N. Miyaura and A. Suzuki, *Chem. Rev.*, 1995, **95**, 2457–2483.
46 46P. Imin, M. Imit and A. Adronov, *Macromolecules*, 2012, **45**, 5045–5050.
47 N. Berton, F. Lemasson, F. Hennrich, M. M. Kappes and M. Mayor, *Chem. Commun.*, 2012, **48**, 2516.
48 P. Imin, M. Imit and A. Adronov, *Macromolecules*, 2011, **44**, 9138–9145.
49 P. Imin, F. Y. Cheng and A. Adronov, *Polym. Chem.*, 2012, **2**, 411–416.
50 T. Okazaki, T. Saito, K. Matsuura, S. Ohshima, M. Yumura and S. Iijima, *Nano Lett.*, 2005, **5**, 2618–2623.
51 F. Schoeppler, C. Mann, T. C. Hain, F. M. Neubauer, G. Privitera, F. Bonaccorso, D. Chu, A. C. Ferrari and T. Hertel, *J. Phys. Chem. C*, 2011, **115**, 14682–14686.
52 S. Heeg, J. T. Abrahamson, M. S. Strano and S. Reich, *Phys. Status Solidi B-Basic Solid State Phys.*, 2012, **249**, 2473–2478.
53 A. Malapanis, V. Perebeinos, D. P. Sinha, E. Comfort and J. U. Lee, *Nano Lett.*, 2013, **13**, 3531–3538.
54 X. Tu, S. Manohar, A. Jagota and M. Zheng, *Nature*, 2009, **460**, 250–253.
55 S. Lebedkin, K. Arnold, O. Kiowski, F. Hennrich and M. M. Kappes, *Phys. Rev. B*, 2006, **73**, 94109.
56 R. Saito, M. Hofmann, G. Dresselhaus, A. Jorio and M. S. Dresselhaus, *Adv. Phys.*, 2011, **60**, 413–550.
57 A. K. Sundramoorthy, S. Mesgari, J. Wang, R. Kumar, M. A. Sk, S. H. Yeap, Q. Zhang, S. K. Sze, K. H. Lim and M. B. Chan-Park, *J. Am. Chem. Soc.*, 2013, **135**, 5569–5581.